

Nonlinear analysis of stability of rock wedges in the abutments of an arch dam due to seismic loading

Hasan Mostafaei^{*1}, Farhad Behnamfar¹ and Mohammad Alembagheri²

¹Department of Civil Engineering, Isfahan University of Technology, Isfahan 8415683111, Iran

²Department of Civil and Environmental Engineering, Tarbiat Modares University, Tehran, Iran

(Received March 1, 2020, Revised November 4, 2020, Accepted November 6, 2020)

Abstract. Investigation of the stability of arch dam abutments is one of the most important aspects in the analysis of this type of dams. To this end, the Bakhtiari dam, a doubly curved arch dam having six wedges at each of its abutments, is selected. The seismic safety of dam abutments is studied through time history analysis using the design-based earthquake (DBE) and maximum credible earthquake (MCE) hazard levels. Londe limit equilibrium method is used to calculate the stability of wedges in abutments. The thrust forces are obtained using ABAQUS, and stability of wedges is calculated using the code written within MATLAB. Effects of foundation flexibility, grout curtain performance, vertical component of earthquake, nonlinear behavior of materials, and geometrical nonlinearity on the safety factor of the abutments are scrutinized. The results show that the grout curtain performance is the main affecting factor on the stability of the abutments, while nonlinear behavior of the materials is the least affecting factor amongst others. Also, it is resulted that increasing number of the contraction joints can improve the seismic stability of dam. A cap is observed on the number of joints, above which the safety factor does not change incredibly.

Keywords: dam; finite element analysis of structures; modeling of structures; non-linear time-series analysis; seismic analysis; structural damage

1. Introduction

Nowadays, a paramount importance is allocated to the safety of concrete arch dams because of the enviro-economic consequences (Hasan *et al.* 2019). The possible overall failure mechanism of this type of dams is opening of contraction joints combined with bending tensile cracking and movement of abutment rock wedges created by foundation joints and discontinuities such as faults, cracks and fractures (Ghanaat 2004).

Concrete arch dams are constructed in individual cantilever monoliths (blocks). To make a solid structure, the vertical contraction joints that separate the blocks from each other are later grouted. These discontinuities are considered as weakness planes under tensile and shear stresses. The contraction joints experience opening and closing cyclic movements during an earthquake where the horizontal tensile stresses are released and forces are redistributed. Opening of these joints creates a different stress distribution, which by transferring forces to the cantilever ultimately leads

*Corresponding author, Ph.D. Candidate, E-mail: h.mostafaei@cv.iut.ac.ir

to increasing compressive stresses. Concrete crushing may appear because of the increased compressive stresses and closed joints.

Some researchers utilized numerical modeling to evaluate the effect of contraction joints behavior on seismic response of arch dams. Dowling and Hall (1989) proposed computation of tensile stresses in the arch direction in the upper portion of the arch dam by the finite element method for linear elastic analysis under earthquake motions. They observed that these stresses are greater than the strength of grouted contraction joints between the adjacent cantilevers. As a result of that, a different cracking pattern and crack opening and sliding responses was determined. Fenves *et al.* (1992) demonstrated that opening of contraction joints had a significant impact on magnitude of stresses under the maximum credible earthquake. They developed a nonlinear element to consider the opening and closing contraction joints, and some factors such as the critical size of the elements, number of contraction joints and the need for using reinforcement in joints, were studied. Ahmadi and Razavi (1992) presented a discrete crack finite element model of the foundation and vertical joints for nonlinear dynamic analysis of concrete arch dams. They showed that vertical joints usually experience tensile failure, shear failure, or both under severe earthquakes and these factors ultimately lead to redistribution of internal stresses. They also estimated the safety factor by calculating the failure load. Lau *et al.* (1998) investigated values of tensile stresses using linear and nonlinear analyses by modeling three contraction joints in arch dams. They showed that the shear strength of the keys and the friction angle of the grouting material had insignificant effects on the behavior of contraction joints. Chuhan demonstrated the non-seismic response of arch dams by considering the reinforcements and contraction joints (Zhang *et al.* 2000). Javanmardi *et al.* (2005) theoretically and experimentally investigated the uplift pressure in seismic cracks induced in concrete dams. Alembagheri and Ghaemian (2016) investigated the seismic behavior of jointed arch dams. They considered a configuration of two joints and showed that considering the contraction joints can increase the seismic safety of the dam. Zeinizadeh *et al.* (2018) studied the effects of hydrodynamic pressures in contraction joints, including waterstops, on the seismic response of high arch dams. They indicated that taking pressure in contraction joints into account leads to significant consequences on the dam behavior. Gua *et al.* (2019) investigated the effect of cantilever and integral loads on seismic behavior of jointed arch dams. They indicated that magnitude and distribution of contraction joint opening are different under these types of loads. Wang *et al.* (2019) studied the nonlinear seismic response of jointed arch dams due to spatially-varying ground motions. They introduced physics-based “rupture-site” approach for predicting the ground motions at dam sites at the MCE level.

Stability of the wedges is another key issue in the design of arch dams in seismically active regions. For this purpose, it is essential to have an appropriate analysis to evaluate stability of the abutment for dam safety. Some researchers have investigated stability of arch dams, including rock wedges in the abutments by different approaches (Chen *et al.* 2003, Goodman and Powell 2003). In Londe (1973) presented a limit equilibrium to evaluate the stability of abutment under thrust and uplift forces. This method incorporated certain assumptions to make the problem static and solvable. These assumptions mainly focus on the mechanics and displacement simplifications, which turn the deformable sliding block to a particle having a single degree of freedom (Liu *et al.* 2013). Nuble and Nuss (2004) investigated the abutment wedge effects on the nonlinear seismic behavior of Morrow Point dam. Their results revealed that the hydrostatic uplift pressures at the dam-foundation interface had a little effect on the peak upstream-downstream displacements. Wang and Li (2007) considered the seismic responses of a high arch dam by an experimental model. The system included the arch dam, contraction joints, and some parts of a reservoir, part of foundation and potential rock

wedges in the abutments, in which the mechanical aspects including uplift pressure on the kinematic planes were carefully simulated. Mills-Bria *et al.* (2008) investigated the nonlinear seismic responses of arch dams considering potential blocks in the foundation using explicit finite element techniques. Sohrabi *et al.* (2009) investigated the stability of the left abutment of Luzzone dam due to seismic loading. They combined the Londe conventional method by the finite element method to evaluate time histories of the safety factor as well as wedge displacements. They assumed that the foundation was a massless medium having a viscous condition at the far-end truncated boundary. Zenz *et al.* (2012) investigated the effect of interaction of wedge and dam on the abutment stability of arch dams. They found that the simplified rigid body method used to carry out the abutment stability analysis under earthquake loading led to a conservative factor of safety. Takaloozadeh and Ghaemian (2014) investigated shape optimization of concrete arch dams considering abutment stability. Wedges in contact with the dam body were considered in their study. They concluded that considering abutment stability could change the optimum shape of the arch dam, and it was a more effective factor than the tensile stresses in the dam body. Mirzabozorg *et al.* (2015) conducted a numerical study to compare the stability of a three-dimensional rock wedge via finite element method and traditional Londe approach. They showed that the limit state Londe method overestimated the wedge displacement in comparison with the finite element method. Mahmoudi *et al.* (2016) investigated the effect of foundation nonlinearity on the seismic response of an existing arch dam. They found that considering foundation nonlinearity had no significant effects on the results due to the special shape of the dam. The results revealed that ignoring reservoir pressure on the foundation overestimated the dam response. Mostafaei *et al.* 2018, Mostafaei *et al.* 2017) calculated the probable wedge displacements of the left bank of Luzzone dam due to seismic loading. They indicated that dynamic analysis was more conservative than quasi-static analysis, and a safety factor of about 1.1 was considered as a limit value, which corresponded to the amount of wedge movement in the dynamic analysis. The Effects of abutment movements on nonlinear seismic response of the arch dam were investigated by Pan and Wang (2019). They indicated that the abutment movement makes damage cracking in the surface outlets and mid-level orifices on the downstream face.

To the authors' best knowledge, there is no study in the literature that investigates the effects of the nonlinear behavior on the stability of arch dam abutments. In the linear analysis, the dam is modeled without the contraction, and peripheral joints, and the material behavior is assumed to be linear. However, because of release of tensile stresses and redistribution of forces, presence of contraction joints as well as the nonlinear behavior of the dam materials can change the seismic response of arch dams and their stability. In this sense, this study focuses on more accurate determination of the loads applied by the arch dam on its wedges, based on the FE model employed, and effects of the mentioned loads on the stability of wedges at the abutments are evaluated.

In the present paper, the Bakhtiari arch dam located in the western part of Iran is subjected to a set of ten real earthquake records. Each record is applied with its three components. The spectral acceleration of the ground motion records is scaled and matched to the target spectrum using the SeismoSignal program. The reservoir is governed by the pressure wave equation, and the reservoir's water is assumed to be compressible. In addition, the foundation is assumed to be a massive medium having viscous boundaries at its truncated far ends. The effects of foundation flexibility, grout curtain performance, vertical component of earthquake, nonlinear behavior of materials, and geometrical nonlinearity on the safety factor of the arch dam against instability are studied.

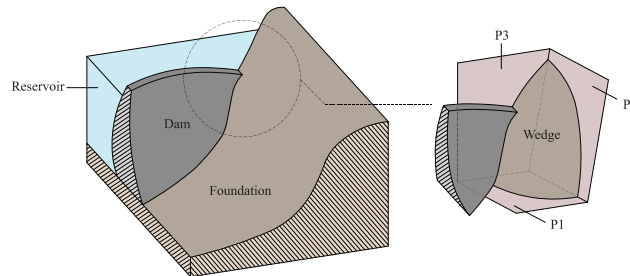


Fig. 1 Dam-reservoir-foundation, wedge and its supporting planes

2. Wedge stability evaluation using the Londe method

On the basis of the Londe method (Londe 1973), the wedge is assumed to be rigid. , in addition, the tensile strength of the wedge 's contact surfaces, the moments of the reaction forces, and their influence on the equilibrium equations are overlooked. The wedges are defined by three probable sliding planes being characterized by their area and orientation (i.e., Dip and Dip direction) owing to solving equilibrium equations (Mostafaei and Behnamfar 2019). The dam, foundation, reservoir, and the typical rock wedge and its supporting planes are shown in Fig. 1. These planes are defined as sub-horizontal ($P1$), and sub-vertical planes ($P2$) and the grout curtain ($P3$), respectively.

To investigate the abutment stability, a 3-D finite element dam-foundation-reservoir model is used, and the thrust forces (F_{TH}^D) are obtained. The other applicable forces on the wedge are categorized as the weight of the wedge (F_w^W), uplift force (F_{Up}^W) due to underground water, and seismic inertial (F_{Eq}^W) force. Water seepage throughout the cracks and fissures of the foundation and the performance of grout curtain exert uplift pressure on the planes of the wedge. The uplift pressure on each plane can be determined by the water level, geometry and area of the plane and the performance of grout curtain. The uplift force on the planes are considered to be constant. Then, the resultant of the applied forces can be calculated as

$$\mathbf{F}_{Res}^W = \mathbf{F}_w^W + \mathbf{F}_{Up}^W + \mathbf{F}_{EQ}^W + \mathbf{F}_{TH}^D \quad (1)$$

Equilibrium equations can be used to obtain the three corresponding normal forces on the planes, which are named as N_1 , N_2 , and N_3 . Since the planes can only be in compression (according to Londe assumptions), emergence of normal tensile forces is a sign of initiation of instability in the shape of sliding or overturning. Different cases of reaction forces and the procedure for calculation of the safety factor (SF) of the wedges against sliding instability are described in the following:

- Case 1: Normal reaction forces on the planes are compressive, which means that the wedge is not detached from any of its supporting planes. Therefore, the wedge is completely stable.
- Case 2: One (and only one) of the reaction forces is calculated to be tensile. Then the wedge will detach from the plane having the tensile reaction force but remain in contact with the two compression planes. Then, occurrence of sliding along the latter planes should be checked. Since this is a concurrent sliding on two planes, a friction force F acting along the common line of the two planes is added to the three translational equilibrium equations and the two unknown reactions and the single friction force are calculated. For instance, if N_3 is tensile, the safety factor is obtained as follows

$$SF = \frac{N_1 \tan(\varphi_1) + c_1 A_1 + N_2 \tan(\varphi_2) + c_2 A_2}{F_{12}} \quad (2)$$

where φ , c and A are respectively friction angle, cohesion and area of the plane with its number appearing as the index. F_{12} is the friction force acting at the intersection of planes 1 and 2.

- Case 3: Two of the reaction forces are tensile. Then sliding can only occur on the third plane. In this case the two tensile reactions are omitted and instead, two normal components of a friction force acting on the third plane along with a normal reaction force, are added and calculated by solving the equilibrium equations. The resultant of the friction force is determined to be F . For example, if N_2 and N_3 are tensile, the safety factor against sliding is obtained as follows:

$$SF = \frac{N_1 \tan(\varphi_1) + c_1 A_1}{F_1} \quad (3)$$

where F_1 is the friction force on the plane 1.

- ❖ Case 4: All the reaction forces are tensile. In this case, the wedge is unstable.

If the safety factor of wedge dropped less than one, the wedge is unstable and will move. The acceleration of the wedge can be obtained as

$$a_{wedge}(t) = \frac{V_w(t) - S_w(t)}{m_w} \quad (4)$$

where $V_w(t)$, $S_w(t)$ and m_w are the driving force, the stabilizing force and mass of the wedge, respectively. Then, the acceleration of wedge is decomposed to the x, y, and z directions. Performing the integration based on the modified Newmark method, velocity and displacement of the wedge can be obtained. It should be noted that the displacement of the wedge is calculates until the sign of velocity changes.

3. Description of the case study

For the purpose of this study, the Bakhtiari double curvature arch dam being 325 m in height (H), 468m in crest length, 5 m in crest thickness, and 54m in base thickness is selected (Dam 2012). It should be noted that the design normal water level is taken as 320m. Moreover, several guidelines, such as FERC (Commission, 1999), and USACE (USACE, 1994, 2007), which have recommended truncated foundation's dimensions are usually considered as being twice as much as the dam height are adopted to reduce the effects of the truncated boundary conditions on the response of the dam. The geometry of the dam-foundation-reservoir system is presented in Fig. 2(a).

3.1 Finite element model

A 3-D finite element model, including dam, reservoir, and foundation is established. Eight-node brick isoparametric element (C3D8R) is used for modeling the concrete dam and its surrounding foundation. The foundation rock is considered to be linearly elastic and the infinite elements are

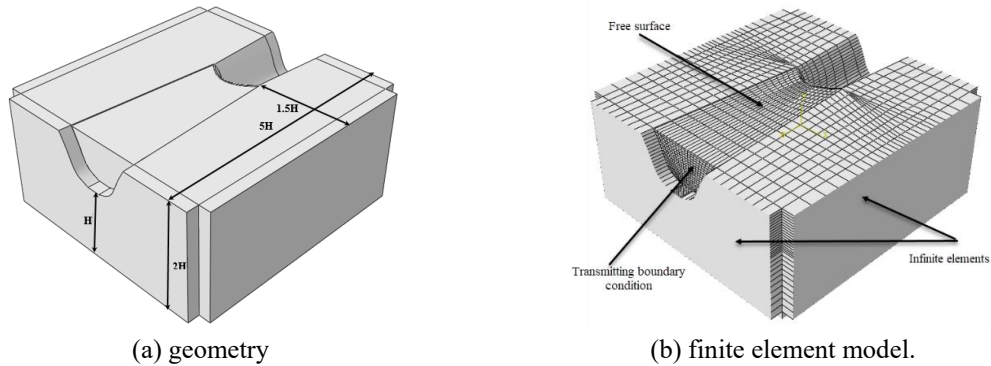


Fig. 2 The dam-foundation-reservoir system of the Bakhtiari dam

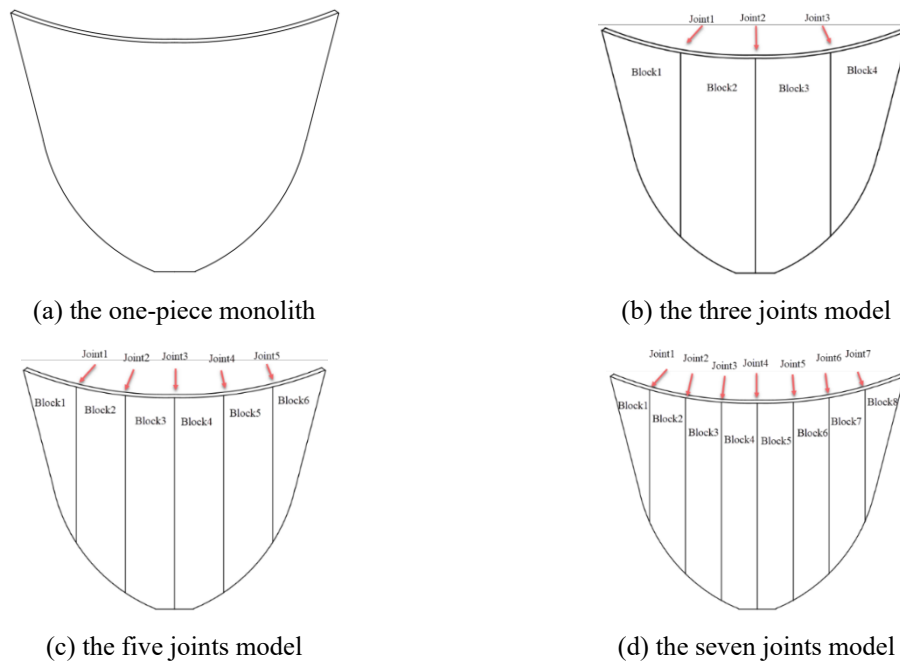


Fig. 3 Dam configurations

utilized at the foundation edges for modeling the radiation damping. Using these elements vanishes the displacement and the stress at infinity. The reservoir water is assumed to be linearly elastic and the acoustic elements (AC3D8R) are used for its modeling. At the far-ends of the reservoir, the transmitting boundary condition is applied. This boundary condition is used to absorb pressure waves going away from the domain. In addition, bottom of the reservoir is assumed to obey a non-absorbing boundary condition. In other word, there is no wave absorption in these boundaries. The current finite element model consists of 1,360, 21,982 and 5,440 elements for the dam, the foundation rock, and the water, respectively. The developed finite element model for the dam, foundation, and reservoir is shown in Fig. 2(b).

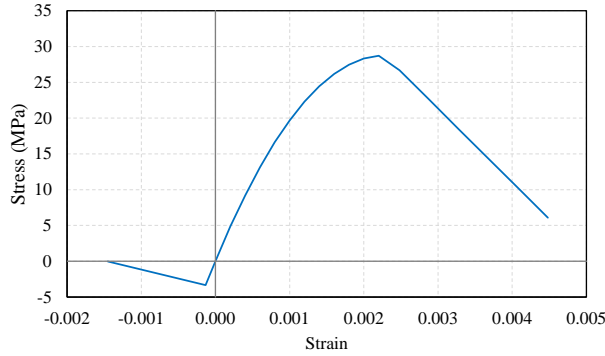


Fig. 4 The Stress-strain model for the tensile and compressive loading of concrete

Four dam configurations are defined: (a) a one-piece monolith, (b) a three-joint model, (c) a five-joint model, and (d) a seven-joint model, as shown in Fig. 3.

The material damping of the dam and foundation is calculated by using the modified Rayleigh damping (Alembagheri and Ghaemian 2013) and the damping ratio is considered to be equal to be 5% of the critical damping. The integrated dam-reservoir-foundation system is considered for obtaining the vibration mode using ABAQUS for carrying out the dynamic analyses (ABAQUS, 2014).

3.2 Material properties

The material parameters of the concrete mass are as follows: modulus of elasticity $E_c = 24GPa$, Poisson's ratio $\nu_c = 0.18$, and mass density of concrete $\rho_c = 2400 kg/m^3$. Since the tension and compression stress-strain response of the test samples are not available, mathematical models are used for this purpose. The concrete constitutive relation under the tensile and compressive loading is defined by employing the Kent and Park model, as seen in Fig. 4.

The nonlinear behavior of concrete is modeled by using the concrete damage plasticity, wherein the tensile cracking and compressive crushing of concrete are considered. Damage variables that are assumed to be functions of inelastic strain can be calculated for these phenomena. The stress-strain relations under uniaxial tension and compression can be expressed as follows

$$\begin{aligned} \sigma_t &= (1 - d_t) E_0 (\varepsilon_t - \varepsilon_t^{pl}) \\ \sigma_c &= (1 - d_c) E_0 (\varepsilon_c - \varepsilon_c^{pl}) \end{aligned} \tag{5}$$

where E_0 is the initial (undamaged) modulus of elasticity, the σ , ε and ε^{pl} are the stress, strain, and inelastic strain of concrete, respectively, in tension (t) and compression (c). Moreover, d_t and d_c are the damage parameters for tensile and compressive, which indicate the degradation of the modulus of elasticity on the strain softening branch of the stress-strain curve. The damage parameter range is from zero to one that zero indicates the undamaged material and one indicates total loss of strength.

The foundation rock domain of the Bakhtiari arch dam is divided into different zones with different modulus of elasticities. The ratio of the foundation elastic modulus (E_f) to that of concrete E_c significantly affects the seismic response of dams (Lin *et al.* 2007). For Bakhtiari arch dam, this ratio changes from 0.145 to 0.792 for different zones. To investigate the effects of the foundation flexibility, the foundation's modulus of elasticity is varied from a quarter to the whole dam concrete's Young's modulus. In addition, the Poisson's ratio and mass density of foundation rock are considered to be $\nu_f = 0.25$ and $\rho_f = 2600 \text{ kg/m}^3$, respectively. The Bulk modulus and mass density of water are assumed to be $K_w = 2.2 \text{ GPa}$ and $\rho_w = 1000 \text{ kg/m}^3$, respectively.

3.3 Contraction joint modeling

By considering stage construction of arch concrete dam, opening of these joints creates large slip and large deformation in monoliths of concrete arch dam (Moradloo *et al.* 2008). Contact between the two surfaces of the contraction joint can have tangential and normal behaviors (Khaneghahi *et al.* 2019). The stresses transmitted across the interfaces, are related to each other by the Coulomb friction model that is defined as follows

$$\tau_u = \mu\sigma \quad (6)$$

where τ_u , σ , and μ are the ultimate shear stress, normal stress and the coefficient of friction, respectively. Also, for modeling the thin layer of the grout material in the contraction joints, the normal behavior of contact is taken to be hard contact condition. In this study, the coefficient of friction is assumed to be 0.6 (Zhang *et al.* 2019).

The delamination at an interface can be modeled with remarkable ease through using the traction-separation constitutive model when the surface-based cohesive behavior being adopted. To be more specific, a linear elastic uncoupled traction-separation law is considered prior to damage that can be written as follows

$$\mathbf{t} = \begin{Bmatrix} t_n \\ t_s \\ t_t \end{Bmatrix} = \begin{bmatrix} K_{nn} & 0 & 0 \\ 0 & K_{ss} & 0 \\ 0 & 0 & K_{tt} \end{bmatrix} \begin{Bmatrix} \delta_n \\ \delta_s \\ \delta_t \end{Bmatrix} = \mathbf{K}\boldsymbol{\delta} \quad (7)$$

where \mathbf{t} , \mathbf{K} and $\boldsymbol{\delta}$ are the nominal traction stress vector, elastic constitutive matrix and separations vector, respectively. Moreover, the subscripts n , s and t are the normal and the two shear directions, respectively. In this study, the tensile strength of joint is considered to be nil as is so often according to the literature (Azmi *et al.* 1998). The normal-stiffness value used for the joints is $K_{nn} = 0$ that make the free separations in their normal directions possible. Moreover, the tangential-stiffness values are considered to be $K_{ss} = K_{tt} = 56 \text{ GPa/m}$ (Azmi and Paultre 2002) for enforcement of the tangential cohesive constraints.

The damage to the cohesive bond can happen following the elastic behavior, providing a damage initiation criterion is met. By neglecting the normal stress, the damage initiation criterion depends on the tangential contact stress state (t_s , and t_t) at the interface. The quadratic stress criterion can be expressed as follows (Zhang *et al.* 2019)

$$\left(\frac{t_s}{t_{s0}} \right)^2 + \left(\frac{t_t}{t_{t0}} \right)^2 = 1 \quad (8)$$

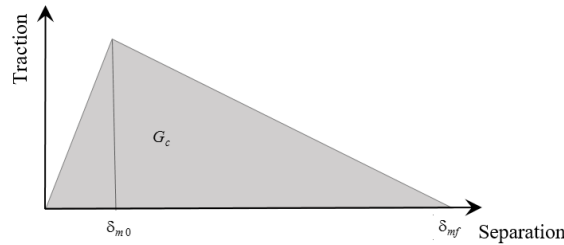


Fig. 5 Linear softening traction-separation law

where t_{s0} , and t_{t0} are the maximum values of the contact stress when the separation is either purely in the first or second shear direction, respectively (Zhang *et al.* 2019). According to contradictory findings in the literatures (Bresler and Pister 1958, Hofbeck *et al.* 1969, Zia 1961), the shear strength of the shear keys is equal to one-tenth the compressive strength of the concrete dam. Therefore, the maximum nominal stresses in the first and second shear directions are taken as 3.0 MPa (i.e., $t_{s0} = t_{t0} = 3.0MPa$) for the damage initiation criterion.

The bond damage process is specified through progressive degradation of the cohesive stiffness when the damage initiation criteria is met. The overall damage at the contact point, D , is calculated by scalar variable between 0 to 1. In what follows, the tangential contact stress components are affected by the damage in the zero-normal-stiffness case.

$$t_s = (1 - D)\bar{t}_s \tag{9}$$

$$t_t = (1 - D)\bar{t}_t \tag{10}$$

where \bar{t}_s , and \bar{t}_t are equal to tangential contact stress components being predicted by the elastic traction-separation behavior for the current separations lack of damage. An efficient separation, δ_m , is introduced to describe the damage evolution under a combination of the two shear-separation components across the interface according to

$$\delta_m = \sqrt{\delta_s^2 + \delta_t^2} \tag{11}$$

After the initiation of damage, a linear softening traction-separation law is considered, as shown in Fig. 5.

The fracture energy, the energy required to forge complete bond failure, is applied for the definition of damage evolution. The area under the traction-separation curve (Fig. 5). Moreover, a quadratic interaction of the energies required to bring about failure in the individual (normal and two shear) directions governs the complete failure as it is given in the following

$$\left(\frac{G_s}{G_{sc}}\right)^2 + \left(\frac{G_t}{G_{tc}}\right)^2 = 1 \tag{12}$$

where G , G_t , G_{sc} , and G_{tc} are the work done by the tractions and their conjugate separations the critical fracture energies required to cause failure in the first and second shear directions, respectively.

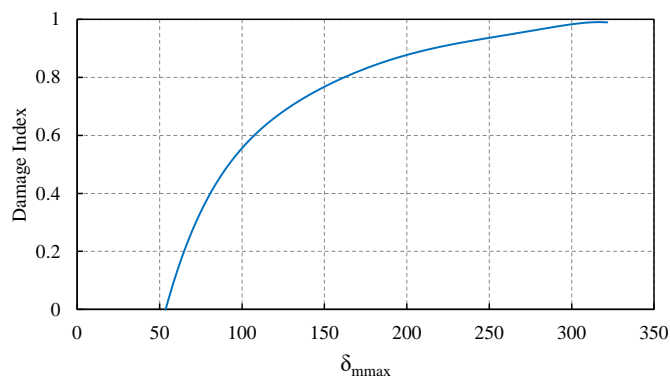


Fig. 6 Damage evolution to the tangential joint cohesion.

Table 1 The unit normal vector of the probable sliding planes (Dam 2012)

| | Sub-horizontal plane (<i>P1</i>) | Sub-vertical planes (<i>P2</i>) | Upstream Plane (<i>P3</i>) |
|------------|------------------------------------|-----------------------------------|------------------------------|
| Left Bank | (0, 0, 1) | (0.332, 0.916, -0.225) | (0.752, -0.606, 0.259) |
| Right Bank | (0, 0, 1) | (-0.484, 0.826, -0.105) | (-0.818, -0.513, 0.259) |

Also, the damage variable's evolution, D , is reduced to

$$D = \frac{\delta_{mf} (\delta_{m \max} - \delta_{m0})}{\delta_{m \max} (\delta_{mf} - \delta_{m0})} \quad (13)$$

where $\delta_{m \max}$ is the peak value of the effective separation during the loading history. The effective separation at damage initiation, δ_{m0} , is estimated to 53.6×10^{-6} m and the effective separation at complete failure, δ_{mf} , is equal to 321.6×10^{-6} m, about six times δ_{m0} . Besides, the fracture energies in the two shear directions being used to define the damage evolution are taken as 0.482×10^{-3} Mpa · m as shown in Fig. 6.

3.4 Wedges definition

The abutment rock wedges are defined by three joint surfaces that intersect at the abutment of the Bakhtiari dam. The unit normal vectors of the probable sliding planes are tabulated in Table 1.

Six wedges have been selected to investigate the stability analysis for each abutment of the dam that are presented in Fig. 7. Two probable sliding planes (*P1* and *P2*) and one back release plane (*P3*) characterize the wedge geometry. *P1* and *P2* planes are referred to sub-horizontal and sub-vertical planes, respectively; and *P3* is located on the upstream side of the wedge, most often considered as the grout curtain. Ultimately, the wedge's shape is completed by the topography surface. The differences among these wedges relate to the location of wedges and the elevation of the horizontal plane. The geometry, shear strength parameters, and uplift force on these discontinuity planes are listed in

Table 2 (Dam 2012). The uplift force is calculated based on the normal level water and area of the plane in the absence of the grout curtain.

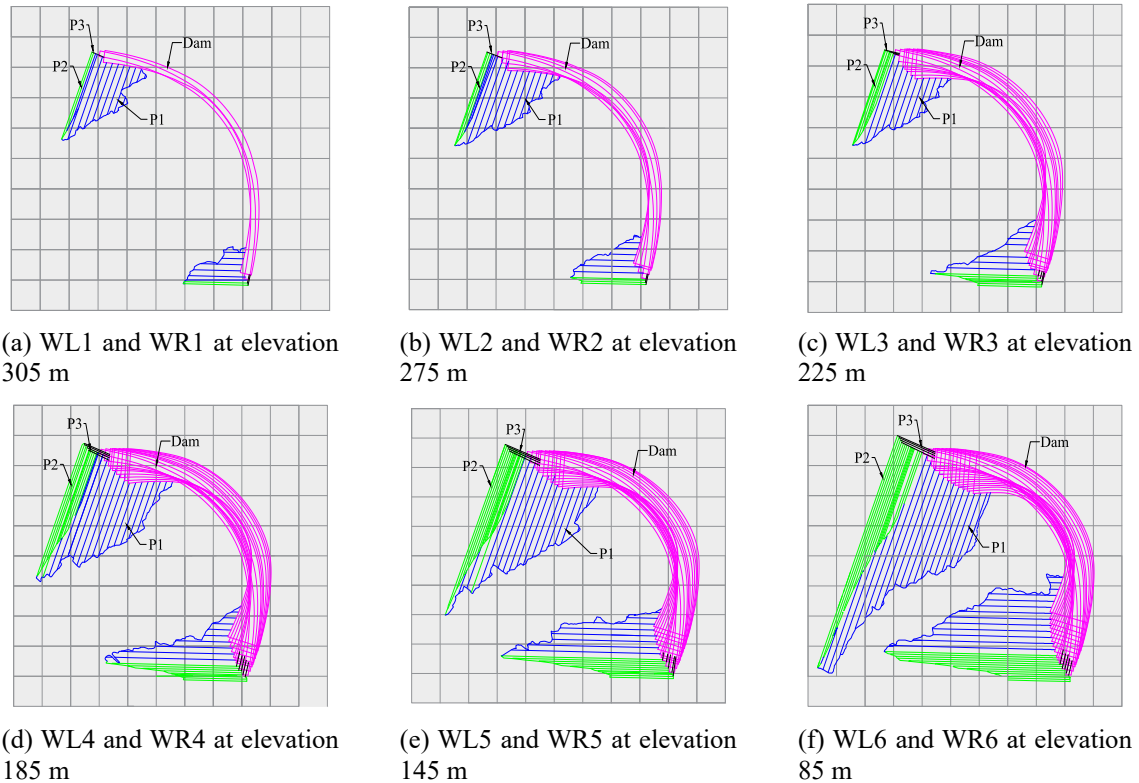


Fig. 7 Geometry of the abutment wedges

3.5 Time-history analysis

To investigate the seismic stability of the wedges, 10 earthquake ground motions are selected in this study extracted from PEER strong-motion database ("PEER strong ground motion database. <<http://peer.berkeley.edu/smcat/search>> ", 2000). For this purpose, the earthquakes recorded on the soil Types A and B (with a shear wave velocity range $V_{s30} \geq 760m/s$), at an intermediate distance of 20–50 km and a magnitude range of 6–7.5 are selected. Considering this criteria, 15 earthquake ground motions are picked up. Then, at most only two records of the same earthquake from various stations retained. These results in 10 earthquake records are listed in Table 3.

Each record contains three components that are applied to the finite element model concurrently. To scale the ground motions, the ASCE/SEI (2016) code is selected. According to this code, the average spectrum of the SRSS response spectra of the horizontal components of the ground motions is calculated. Such a spectrum is scaled such that it does not fall below 90% of the design spectrum anywhere between $0.2 T$ to $2T$ where T is the fundamental period of the system. The design spectrum and the average response spectrum before and after scaling are shown in Fig. 8. The fundamental period of system appears to be 1.428 sec. Then, the scale factor at the DBE level emerges to be 2.89 the corresponding value at the MCE level is assumed to be 1.5 times larger, i.e., 4.335.

Table 2 Geometrical and mechanical characteristics of the wedges (Dam 2012)

| Wedge | Sub-Horizontal Plane (P1) | | | | Sub-Vertical Plane (P2) | | | | Upstream Plane (P3) | | | | Elevation | | |
|------------|---------------------------|---------|------------|------------------------|-------------------------|---------|------------|------------------------|---------------------|---------|------------|------------------------|-----------|--------------------------------|-----------|
| | Uplift Force (MN) | C (MPa) | Φ (°) | Area (m ²) | Uplift Force (MN) | C (MPa) | Φ (°) | Area (m ²) | Uplift Force (MN) | C (MPa) | Φ (°) | Area (m ²) | From-to | Wedge volume (m ³) | |
| Left bank | WL1 | 58 | 0.3 | 45.3 | 3,800 | 253 | 0 | 32 | 2,273 | 75 | 0.3 | 45 | 275 | 305-325 | 62,258 |
| | WL2 | 421 | 0.3 | 44.5 | 4,991 | 1117 | 0.1 | 42 | 5,934 | 394 | 0.3 | 45 | 902 | 275-325 | 194,096 |
| | WL3 | 1168 | 0.4 | 43.5 | 6,591 | 4744 | 0.1 | 42 | 13,754 | 1812 | 0.3 | 45 | 2451 | 225-325 | 424,886 |
| | WL4 | 2576 | 0.5 | 43.1 | 10,112 | 10893 | 0.1 | 42 | 22,655 | 4033 | 0.3 | 45 | 4103 | 185-325 | 744,914 |
| | WL5 | 5724 | 0.5 | 42.7 | 14,784 | 21258 | 0.1 | 42 | 34,561 | 7460 | 0.3 | 45 | 6069 | 145-325 | 1,251,255 |
| | WL6 | 11432 | 0.6 | 42 | 23,514 | 39453 | 0.1 | 42 | 54,974 | 14042 | 0.3 | 45 | 9720 | 85-325 | 2,396,494 |
| Right bank | WR1 | 250 | 0.3 | 45.3 | 9,003 | 343 | 0 | 32 | 2,987 | 105 | 0.3 | 45 | 339 | 305-325 | 141,808 |
| | WR2 | 1209 | 0.3 | 44.6 | 12,445 | 1447 | 0.1 | 42 | 7,834 | 623 | 0.3 | 45 | 1304 | 275-325 | 464,062 |
| | WR3 | 5128 | 0.4 | 44 | 18,657 | 5543 | 0.1 | 42 | 17,160 | 3260 | 0.3 | 45 | 4096 | 225-325 | 1,089,998 |
| | WR4 | 9857 | 0.4 | 43.4 | 24,349 | 11503 | 0.1 | 42 | 26,093 | 7724 | 0.3 | 45 | 7354 | 185-325 | 1,949,327 |
| | WR5 | 17212 | 0.6 | 41.4 | 30,584 | 21397 | 0.1 | 42 | 37,036 | 15002 | 0.3 | 45 | 11476 | 145-325 | 3,042,590 |
| | WR6 | 37687 | 0.5 | 42.4 | 46,244 | 42357 | 0.1 | 42 | 60,159 | 29315 | 0.3 | 45 | 19407 | 85-325 | 5,317,911 |

Table 3 Characteristics of the earthquake records selected

| No. | Earthquake | RSN number | Magnitude (M) | Year | Un-scaled PGA (g) | | |
|------|-----------------|------------|---------------|------|-------------------|--------------|----------|
| | | | | | Stream | Cross-stream | Vertical |
| EQ1 | San Fernando | 80 | 6.61 | 1971 | 0.095 | 0.205 | 0.089 |
| EQ2 | Morgan Hill | 476 | 6.19 | 1984 | 0.039 | 0.076 | 0.031 |
| EQ3 | N. Palm Springs | 511 | 6.06 | 1986 | 0.098 | 0.119 | 0.066 |
| EQ4 | N. Palm Springs | 536 | 6.06 | 1986 | 0.114 | 0.086 | 0.049 |
| EQ5 | Northridge-01 | 1011 | 6.69 | 1994 | 0.103 | 0.159 | 0.105 |
| EQ6 | Northridge-01 | 1091 | 6.69 | 1994 | 0.151 | 0.139 | 0.091 |
| EQ7 | Tottori Japan | 3925 | 6.61 | 2000 | 0.128 | 0.185 | 0.125 |
| EQ8 | Iwate | 5483 | 6.9 | 2008 | 0.066 | 0.085 | 0.039 |
| EQ9 | Iwate | 5680 | 6.9 | 2008 | 0.152 | 0.227 | 0.127 |
| EQ10 | San Simeon CA | 8167 | 6.52 | 2003 | 0.047 | 0.034 | 0.021 |

For each dynamic analysis, the applied static loads including the deadweight and the hydrostatic load are exerted and afterwards all three components of scaled ground earthquakes are excited simultaneously at the dam–foundation interface as excitation based on the free field model (Yu *et al.* 2019).

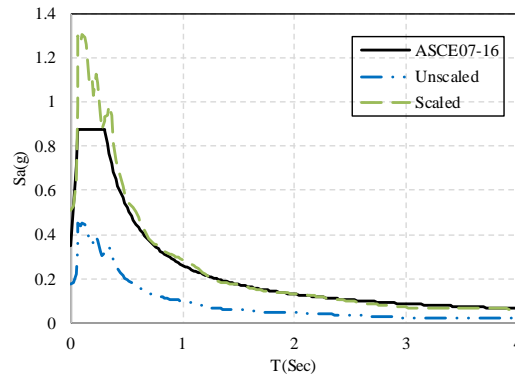


Fig. 8 Scaling of average response spectrum, for the DBE hazard level.

4. Results and discussion

As stated in section 3, the applied forces on the wedge are categorized as weight of the wedge, uplift force, seismic inertia force, and the thrust force. The analysis is conducted using ABAQUS to compute thrust forces that act on the wedges, and other forces (weight, water pressures, inertia, etc.) are also accounted for, using a MATLAB Program. The foundation flexibility, vertical component of earthquake, nonlinear behavior of materials, and geometrical nonlinearity are important parameters affecting the thrust forces. In this study, the effective parameters on the thrust forces, vertical component of the earthquake, and the effect of grout curtain performance on the stability of the dam abutments are focused on to identify the main affecting factors.

Four values are taken for the ratio of the modulus of elasticity of foundation rock E_f to that of concrete E_c to investigate the effect of foundation flexibility; the mentioned values are 0.25, 0.5, 0.75, and 1.

In addition, linear and nonlinear analysis are conducted separately for obtaining the thrust forces. In the linear analysis, the dam body is considered to be a one-piece monolith, and the material behavior is assumed to be linear while in nonlinear analysis, the discontinuity in the dam body due to the contraction joints is considered and the concrete material behavior is nonlinear.

Two hazard levels, DBE and MCE, are considered to investigate the effects of earthquake severity on the stability of the dam abutments. Also, to study the effect of the vertical component, in time history analysis, first the vertical component of the ground motion is ignored and the responses are compared with when it is presented.

One of the most important steps in designing dams is the sealing of foundation and abutments. The most common method of sealing is the injection of cement-based grouts. The main purposes of the implementing of the grout curtain are: decreasing the seepage rate to the acceptable limit and increasing the dam safety (Mostafaei *et al.* 2017). The performance of the grout curtain depends on various parameters such as the rock permeability, borehole spacing, and density and the pressure of grout. The observation of seepage and uplift problems is possible just after the first impounding in the numerous dams through abutments (Aghda *et al.* 2019, Khan *et al.* 2011). Based on the performance of the grout curtain, the uplift force is as a percentage of the values that are calculated in the absence of the grout curtain (See Table 2). To investigate effect of the uplift forces, as indicated in Table 4, two uplift distributions are assumed in the stability analysis of each defined wedge. The

uplift pressure on the grout curtain plane is considered to be in its full value, and those on the two other planes are considered to be in two different cases, namely low pressure (LP) and high pressure (HP), that relates to the extent of imperfection presumed for the grout curtain.

In section 4.1- 4.3, effect of the material nonlinearity is disregarded.

The thrust forces can be obtained through the summation of abutment nodes forces. The time histories of the thrust forces applied on WL6 wedge at the left abutment due to EQ9 at the DBE level are shown in Fig. 9.

Fig. 10 shows the safety factor of WL6 wedge at the left abutment due to EQ9 at the DBE level. It can be seen from Fig. 6 that the wedge is unstable for some periods of time. It should be noted that since the safety factor of wedge dropped less than one, the reaction values was not be accurate.

The time histories of calculated displacements of WL6 at the left abutment due to EQ9 at the DBE level for different uplift pressure distribution are presented in Fig. 11.

Fig. 11 indicates that the wedge displacement rises, as the uplift pressure distribution increases. It should be noted that these displacements can lead to higher stresses in dam body. It should be pointed out that the absolute deformation of foundation and abutments are determined by using extensometers (Ziaei *et al.* 2017). The minimum of the safety factor of wedges due to different earthquakes are presented in Table 5 when $E_f/E_c = 0.5$ and low-pressure distribution is applied on the planes. Table 5 indicates that the location of the bed rock has significant effect on the stability of arch dam abutments. It should be noted that the minimum safety factor occurs in WL6 wedge at the left abutment at the DBE level, when $E_f/E_c = 0.5$ and low uplift pressure distribution.

Table 4 Uplift pressure distributions

| Uplift distribution | P1 | P2 | P3 |
|---------------------|-----|-----|------|
| LP | 33% | 33% | 100% |
| HP | 66% | 66% | 100% |

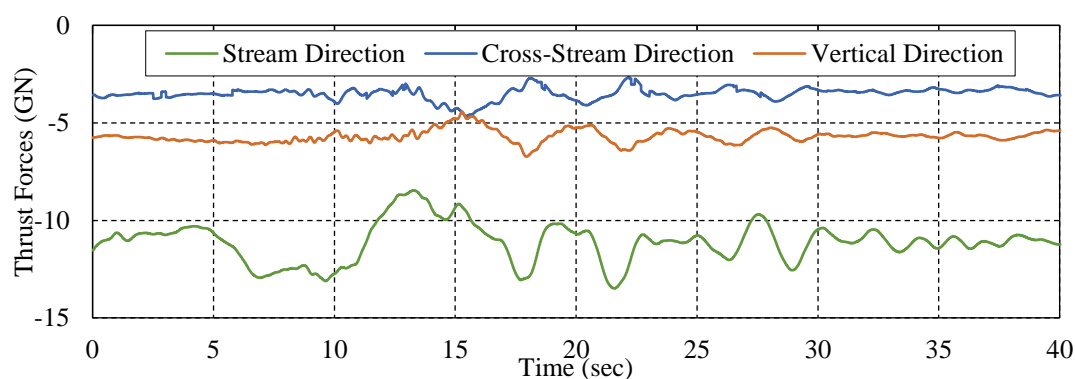


Fig. 9 The time histories of thrust forces of WL6 at the left abutment due to EQ9 for the DBE level and $E_f/E_c = 0.5$

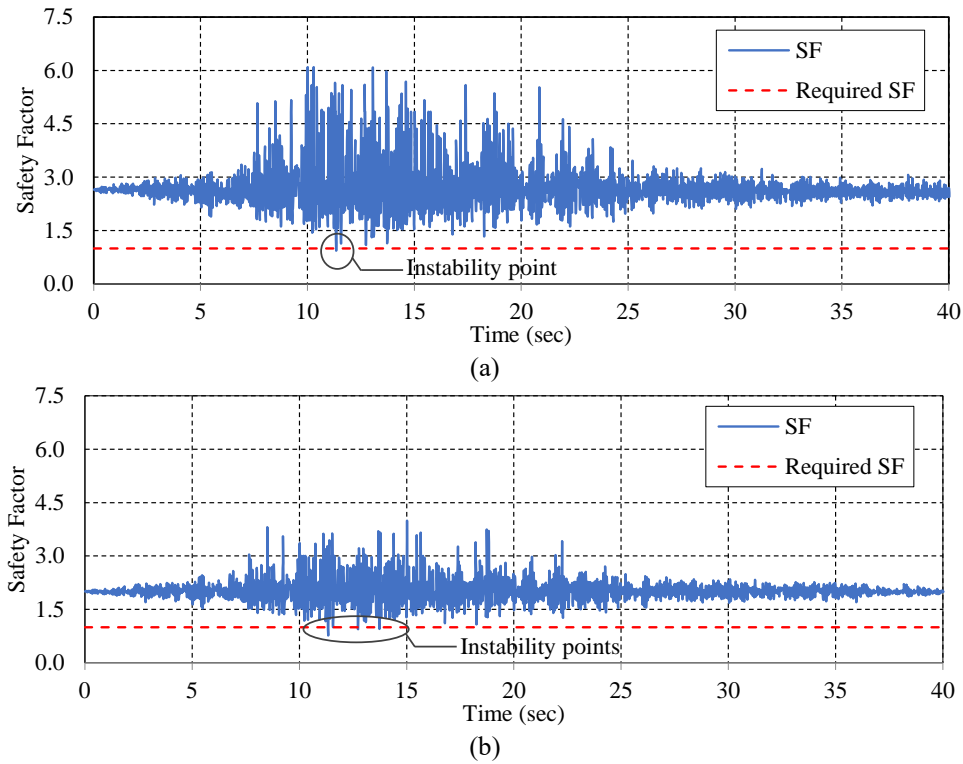


Fig. 10 The time histories of safety factors of WL6 at the left abutment due to EQ9 at the DBE level and $E_f/E_c = 0.5$. (a) low uplift pressure distribution and (b) high uplift pressure distribution

Table 5 The minimum safety factor of wedges at the DBE level for $E_f/E_c = 0.5$ and low uplift pressure distribution

| Wedge | EQ1 | EQ2 | EQ3 | EQ4 | EQ5 | EQ6 | EQ7 | EQ8 | EQ9 | EQ10 | Mean | |
|------------|------|-------|-------|-------|-------|-------|-------|-------|-------|-------|-------|-------|
| Left bank | WL1 | 2.68 | 4.65 | 4.00 | 4.68 | 2.72 | 2.77 | 2.43 | 4.32 | 2.14 | 6.06 | 3.65 |
| | WL2 | 2.00 | 3.59 | 2.65 | 3.27 | 2.19 | 1.68 | 2.00 | 3.24 | 1.34 | 4.69 | 2.66 |
| | WL3 | 1.42 | 2.11 | 1.76 | 2.03 | 1.43 | 1.28 | 1.32 | 1.97 | 1.11 | 2.25 | 1.67 |
| | WL4 | 1.30 | 1.90 | 1.56 | 1.80 | 1.32 | 1.11 | 1.19 | 1.77 | 1.01 | 1.96 | 1.49 |
| | WL5 | 1.26* | 1.85* | 1.48* | 1.71* | 1.25* | 1.02* | 1.14* | 1.70* | 0.94 | 1.86* | 1.42* |
| | WL6 | 1.31 | 1.95 | 1.52 | 1.77 | 1.26 | 1.03 | 1.19 | 1.79 | 0.93* | 1.96 | 1.47 |
| Right bank | WR1 | 3.86 | 9.31 | 4.35 | 7.05 | 4.85 | 3.11 | 3.98 | 9.39 | 2.83 | 13.20 | 6.19 |
| | WR2 | 2.45 | 5.81 | 3.06 | 4.18 | 3.10 | 2.10 | 2.62 | 5.87 | 1.95 | 11.94 | 4.31 |
| | WR3 | 2.17 | 5.41 | 2.80 | 3.47 | 2.63 | 1.97 | 2.28 | 4.87 | 1.78 | 7.57 | 3.49 |
| | WR4 | 1.86 | 4.28 | 2.47 | 2.77 | 2.18 | 1.71 | 1.96 | 3.70 | 1.60 | 5.08 | 2.76 |
| | WR5 | 1.62 | 3.32 | 2.24 | 2.29 | 1.90 | 1.58 | 1.79 | 2.87 | 1.51 | 3.36 | 2.25 |
| | WR6 | 1.40 | 2.49 | 1.96 | 1.77 | 1.52 | 1.28 | 1.47 | 2.07 | 1.31 | 2.09 | 1.74 |
| Minimum | 1.26 | 1.85 | 1.48 | 1.71 | 1.25 | 1.02 | 1.14 | 1.70 | 0.93 | 1.86 | 1.42 | |

*The critical wedge

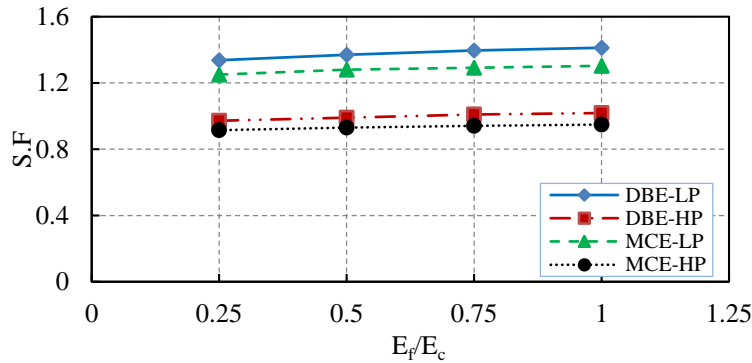


Fig. 12 Comparison of the mean of minimum safety factor of wedges for different values of modulus of elasticity ratio, and the uplift pressure distribution

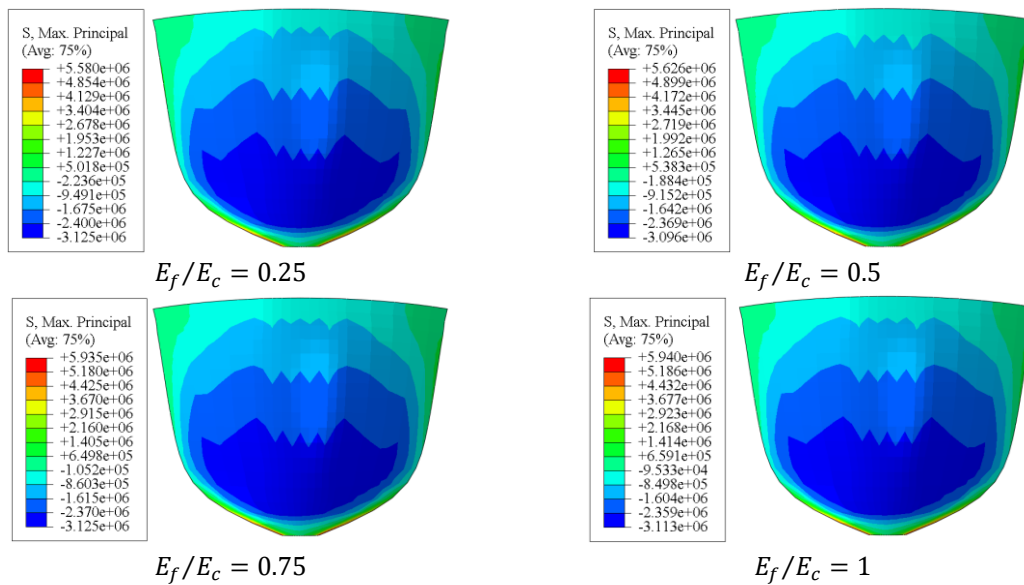


Fig. 13 Stress contours of dam due to EQ9 at the DBE level for different values of modulus of elasticity ratio

It can be seen from the table that the wedges at left abutment are more critical than those in right abutment. It is mainly due to the reality that the wedges on the left bank of the dam are smaller in volume than others.

4.1 Foundation flexibility

The effects of foundation flexibility on the minimum safety factor (S.F) is shown in Fig. 12 under both DBE and MCE ground motion levels.

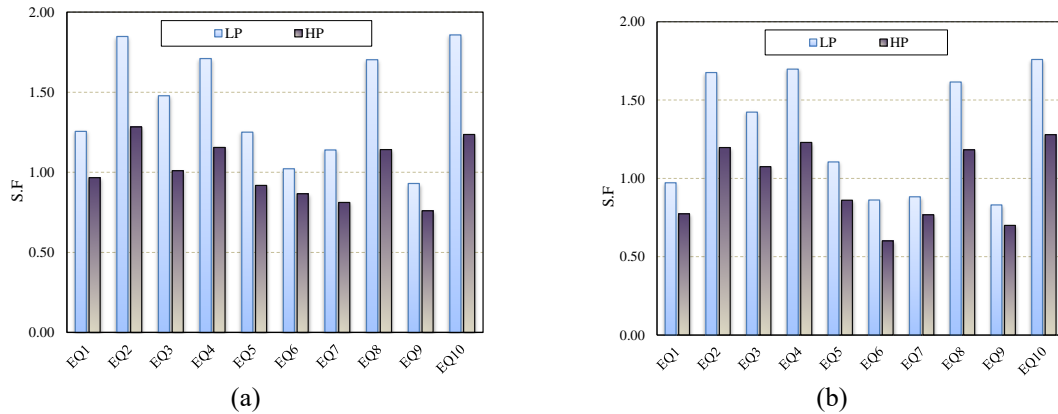


Fig. 14 Comparison of the minimum safety factor of wedges between two uplift pressure distributions (See Table 5) for $E_f/E_c = 0.5$. (a) DBE ground motion level (b) MCE ground motion level.

According to Fig. 12, the safety factor of dam abutments slightly increases by increasing the foundation rigidity. To investigate this behavior further, the stress contours of the dam at the moment that the safety factor is minimum are shown in Fig. 13 under EQ9 at DBE level for different values of modulus of elasticity ratio. As observed, the maximum principal stresses decrease at smaller values of the foundation’s modulus of elasticity. The maximum principal stress happens at the base of the dam. It decreases by 20% for a softer rock. On this account, magnitude of the thrust forces decreases, and the possibility of wedge sliding on its supporting planes increases.

The results indicate that the stress contour of the dam rises significantly, as the foundation flexibility decreases. However, the foundation flexibility has a weak influence on the stability of dam abutments.

4.2 Grout curtain efficiency

Fig. 14 shows the effect of uplift pressure distribution on the stability of the wedges under different ground motion levels. This figure shows that increase of the uplift pressure decreases the minimum safety factor of the dam under both ground motion levels. This phenomenon can destabilize the system since the average of the minimum safety factors is less than one as it equals 0.99 and 0.93 at the DBE and MCE levels, respectively.

According to Fig. 14, on average, deterioration of efficiency of the grout curtain corresponding to HP results in reduction of the safety factor up 28.1% and 24.2% at the DBE and MCE levels, respectively.

4.3 Effect of the vertical component of the ground motions

Fig. 15 indicates effect of the vertical component of the earthquakes on the safety factor of wedges at the DBE and MCE levels. As expected, eliminating the vertical component of ground motion increases the safety factor. This is due to the fact that in absence of the vertical component, the normal stresses can increase along the contact planes that results in more stability. In the presence of the vertical component, the safety factor decreases to 9.45% on average.

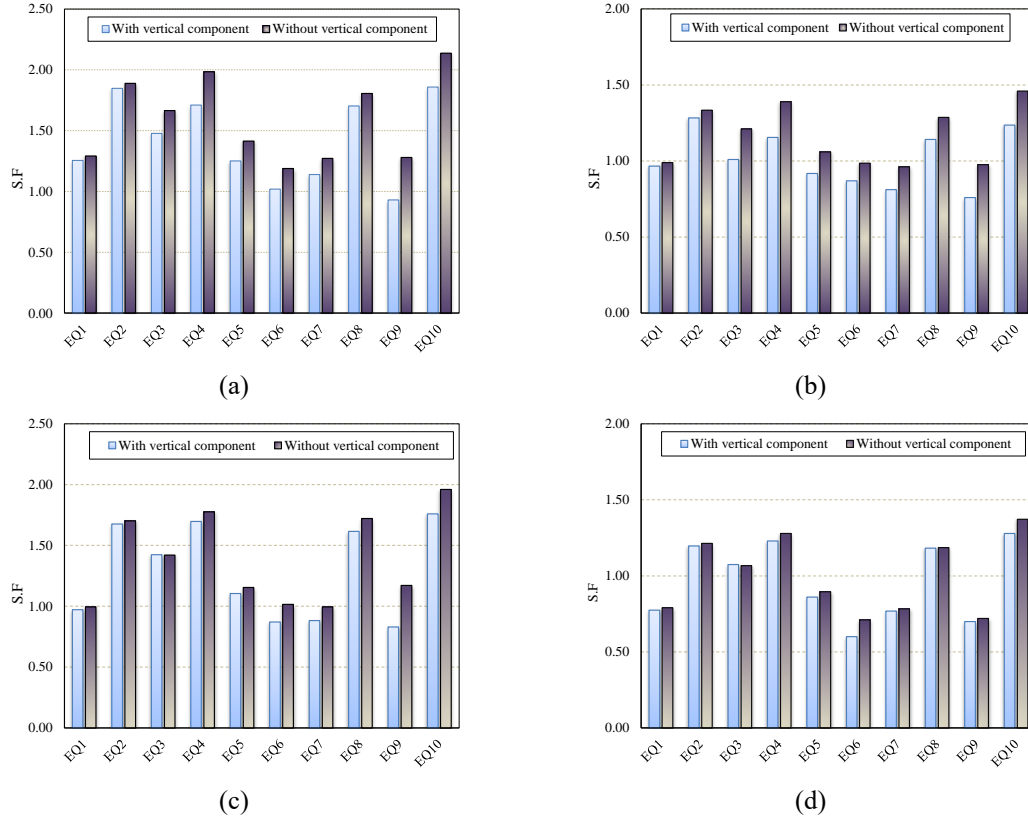


Fig. 15 Comparison of the minimum safety factor of wedges with and without presence of the vertical component of the earthquake for $E_f/E_c = 0.5$. (a) LP at DBE level (b) LP at MCE level (c) HP at DBE level (d) HP at MCE level. (See Table 5)

Table 6 Comparison of the average of the minimum safety factor of wedges between cases of with and without vertical component for $E_f/E_c = 0.5$

| Hazard Level | LP | | | HP | | |
|---------------------------------|-------------------------|----------------------------|---------------------------------------|-------------------------|----------------------------|---------------------------------------|
| | With vertical component | Without vertical component | Difference for vertical component (%) | With vertical component | Without vertical component | Difference for vertical component (%) |
| DBE | 1.37 | 1.53 | 11.7 | 0.99 | 1.13 | 11.1 |
| MCE | 1.28 | 1.39 | 8.6 | 0.93 | 0.98 | 6.4 |
| Difference for hazard level (%) | 7 | 10 | --- | 6 | 15.3 | --- |

Table 7 Comparison of the minimum safety factor of wedges for linear and nonlinear analysis for $E_f/E_c = 0.5$

| Hazard Level | Uplift pressure | Type of analysis | EQ1 | EQ2 | EQ3 | EQ4 | EQ5 | EQ6 | EQ7 | EQ8 | EQ9 | EQ10 | Mean |
|--------------|-----------------|------------------|------|------|------|------|------|------|------|------|------|------|------|
| DBE | Low | Linear | 1.26 | 1.85 | 1.48 | 1.71 | 1.25 | 1.02 | 1.14 | 1.70 | 0.93 | 1.86 | 1.37 |
| | | Nonlinear | 1.26 | 1.85 | 1.48 | 1.71 | 1.25 | 1.02 | 1.14 | 1.70 | 0.93 | 1.85 | 1.37 |
| | High | Linear | 0.97 | 1.28 | 1.01 | 1.15 | 0.92 | 0.87 | 0.81 | 1.14 | 0.76 | 1.24 | 0.99 |
| | | Nonlinear | 0.97 | 1.28 | 1.01 | 1.15 | 0.92 | 0.87 | 0.81 | 1.14 | 0.76 | 1.23 | 0.99 |
| MCE | Low | Linear | 0.97 | 1.68 | 1.42 | 1.70 | 1.10 | 0.87 | 0.88 | 1.62 | 0.83 | 1.76 | 1.28 |
| | | Nonlinear | 0.97 | 1.68 | 1.42 | 1.70 | 1.09 | 0.86 | 0.88 | 1.61 | 0.83 | 1.51 | 1.25 |
| | High | Linear | 0.77 | 1.20 | 1.07 | 1.23 | 0.86 | 0.60 | 0.77 | 1.18 | 0.70 | 1.28 | 0.93 |
| | | Nonlinear | 0.77 | 1.20 | 1.07 | 1.23 | 0.85 | 0.60 | 0.77 | 1.18 | 0.70 | 1.18 | 0.92 |

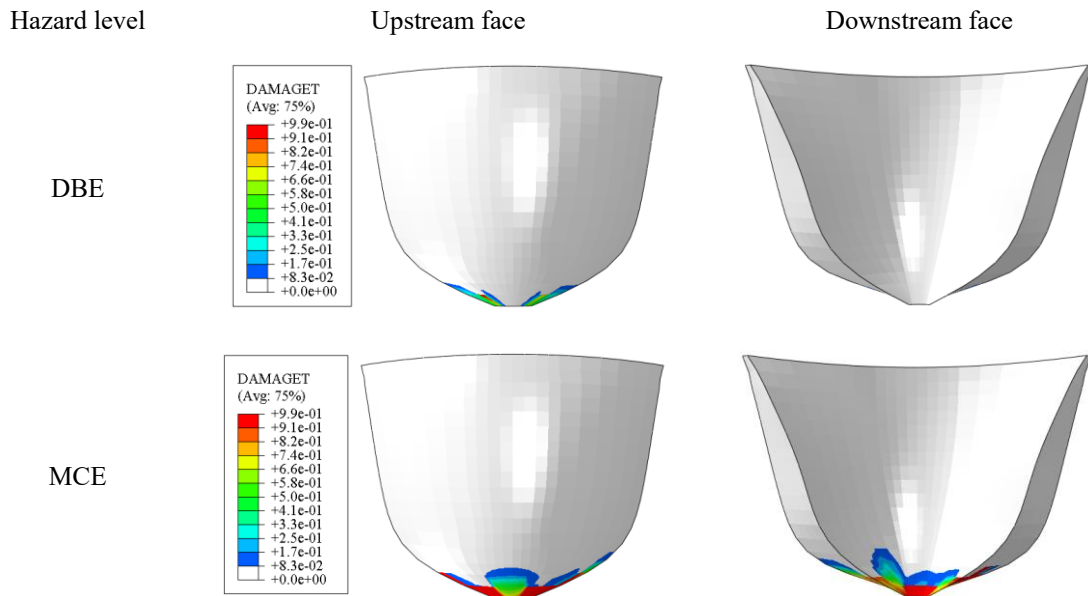


Fig. 16 Tensile damage contours of dam due to EQ9 at the DBE and MCE hazard levels

The averages of the minimum safety factor of wedges with and without vertical component of ground motions are listed in Table 6 for different hazard levels and the uplift distribution pressure. It is observed that the smaller values of the safety factor correspond to the MCE level when the vertical component is present and the uplift pressure is higher.

4.4 Effect of material nonlinearity

A comparison between the linear and nonlinear analysis is made to scrutinize the effects of material nonlinearity on the minimum safety factor of wedges at DBE and MCE levels as shown in Table 7.

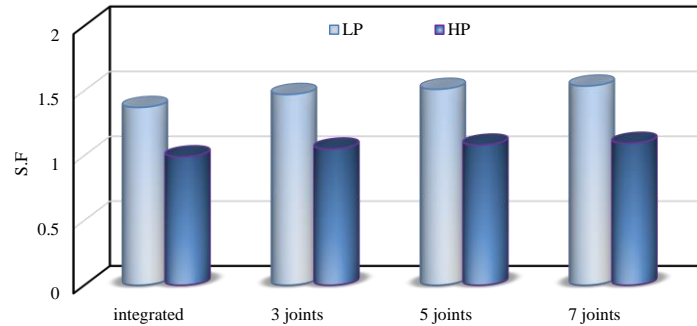


Fig. 17 The average of minimum safety factor of the wedges for different numbers of contraction joint for $E_f/E_c = 0.5$ and uplift pressure distribution

Individual as well as mean values of the safety factors reported in Table 7 show that no important material nonlinearity happens in the system even at the MCE level. Therefore, it is not necessary to be taken into account in the safety factor analysis. Fig. 16 indicates the tensile damage contours of the dam due to EQ9 at the DBE and MCE hazard levels.

As observed, the base of the dam is the first region that experiences damage, and by increasing the severity of the earthquakes, damages propagate toward the abutments. Given the location of the wedges, these damages have a slight effect on the stability of the abutment, and as the severity of the earthquake increases, this effect is increased.

4.5 Effect of Geometric nonlinearity

Fig. 17 shows effect of the contraction joints and their numbers on the average of the minimum safety factor of wedges.

Fig. 17 indicates that the contraction joints increase the safety factor of the wedge, and by increasing their number, the safety factor exhibits an asymptotic behavior. Opening and closing of these joint increases the compressive stresses in the dam, but does not change the tensile stresses. Therefore, they improve the seismic resistance of the dam structure, and the thrust forces press the wedge to its supporting planes, and the seismic safety of abutments increase.

5. Conclusions

In this research, seismic stability of the Bakhtiari arch dam was investigated using time history analysis. Presence of six wedges at each abutment of the dam was assumed for the analysis. A 3-D finite element model of the dam was utilized, including the dam body, its foundation, and reservoir, to compute the thrust forces. Safety factor of the wedges against sliding instability was calculated based on the Londe method. The effects of foundation flexibility, grout curtain performance, vertical component of earthquake, nonlinear behavior of concrete material, and geometrical nonlinearity of contraction joints on the safety factor were investigated.

The prime results of this research are as follows:

- 1) The location of the bed rock plays a key role in the stability of arch dam abutments.

- 2) By decreasing flexibility of the foundation rock, the stress contour of the dam rises considerably, while the minimum safety factor of the wedges increases lightly.
- 3) Taking of the vertical component of ground motion into account resulted in 11.7% and 11.1% decrease in the safety factor at the DBE and MCE levels for low distribution of the uplift pressure, respectively.
- 4) Overall, the amount of material nonlinearity was insignificant even at the MCE level of seismic hazard. Therefore, the stability analysis can be performed ignoring the concrete material nonlinearity.
- 5) Contrary to the material nonlinearity, it is important to consider the geometrical nonlinearity at the contraction joints by limiting transfer of tensile stresses. This resulted in 7.2% increase in the safety factor because of redistribution of stresses between the arch and cantilever actions.
- 6) The main factor affecting the dam stability was recognized to be distribution of the uplift pressure. Increase of the uplift pressure decreases the minimum safety factor of the abutments under both of the DBE and MCE ground motion levels. Therefore, it is essential to have a realistic estimation of the uplift pressure when performing seismic analysis.

References

- ABAQUS. (2014), Analysis User's Manual Version 6.14. *Dassault Systems*.
- Aghda, S.M.F., GanjaliPour, K. and Esmaeilzadeh, M. (2019), "The Effect of Geological Factors on the Grout Curtain Performance Analysis of Darian Dam Using the Results of Instrumentation Data in the First Impounding", *J. Geolog. Soc. India*, **93**(3), 360-368.
- Ahmadi, M. and Razavi, S. (1992), "A three-dimensional joint opening analysis of an arch dam", *Comput. Struct.*, **44**(1-2), 187-192.
- Alembagheri, M. and Ghaemian, M. (2013), "Damage assessment of a concrete arch dam through nonlinear incremental dynamic analysis", *Soil Dynam. Earthq. Eng.*, **44**, 127-137.
- Alembagheri, M. and Ghaemian, M. (2016), "Seismic performance evaluation of a jointed arch dam", *Struct. Infrastruct. Eng.*, **12**(2), 256-274.
- Azmi, M. and Paultre, P. (2002), "Three-dimensional analysis of concrete dams including contraction joint non-linearity", *Eng. Struct.*, **24**(6), 757-771.
- Bresler, B. and Pister, K.S. (1958), *Strength of concrete under combined stresses*, Paper presented at the Journal Proceedings.
- Chen, S.H., Xu, M.Y., Shahrou, I. and Egger, P. (2003), "Analysis of arch dams using coupled trial load and block element methods", *J. Geotech. Geoenviron. Eng.*, **129**(11), 977-986.
- Commission, F.E.R. (1999), Engineering guidelines for the evaluation of hydropower projects. Chapter 11- Arch Dams. *Washington DC, 20426*, 11-18.
- Dam, B.H. (2012), *Preliminary Stability Analysis of Abutments*. Retrieved from
- Dowling, M.J. and Hall, J.F. (1989), "Nonlinear seismic analysis of arch dams", *J. Eng. Mech.*, **115**(4), 768-789.
- Fenves, G.L., Mojtahedi, S. and Reimer, R.B. (1992), "Effect of contraction joints on earthquake response of an arch dam", *J. Struct. Eng.*, **118**(4), 1039-1055.
- Ghanaat, Y. (2004), *Failure modes approach to safety evaluation of dams*. Paper presented at the 13th world Conference on Earthquake Engineering, Vancouver, Canada
- Goodman, R.E. and Powell, C. (2003), "Investigations of blocks in foundations and abutments of concrete dams", *J. Geotech. Geoenviron. Eng.*, **129**(2), 105-116.
- Guo, S., Liang, H., Li, D., Chen, H. and Liao, J. (2019), "A Comparative Study of Cantilever-and Integral-Type Dead Loads on the Seismic Responses of High Arch Dams", *Int. J. Struct. Stab. Dynam.*, **19**(3),

- 1950021.
- Hofbeck, J., Ibrahim, I. and Mattock, A.H. (1969), *Shear transfer in reinforced concrete*, Paper presented at the Journal Proceedings.
- Javanmardi, F., Léger, P. and Tinawi, R. (2005), "Seismic water pressure in cracked concrete gravity dams: experimental study and theoretical modeling", *J. Struct. Eng.*, **131**(1), 139-150.
- Khan, M.S., Gilani, T.A. and Gul, M.A. (2011), "Post impounding problems and management measures in carbonate geology at Khanpur dam project", Pakistan. *Science International (Lahore)*, **23**(2), 129-134.
- Khaneghahi, M.H., Alembagheri, M. and Soltani, N. (2019), "Reliability and variance-based sensitivity analysis of arch dams during construction and reservoir impoundment", *Front. Struct. Civil Eng.*, **13**(3), 526-541.
- Lau, D.T., Noruziaan, B. and Razaqpur, A. (1998), "Modelling of contraction joint and shear sliding effects on earthquake response of arch dams", *Earthq. Eng. Struct. D.*, **27**(10), 1013-1029.
- Lin, G., Du, J. and Hu, Z. (2007), "Earthquake analysis of arch and gravity dams including the effects of foundation inhomogeneity", *Frontiers of Architecture and Civil Engineering in China*, **1**(1), 41-50.
- Liu, Y.R., He, Z., Leng, K.D., Huang, Y.Q. and Yang, Q. (2013), "Dynamic limit equilibrium analysis of sliding block for rock slope based on nonlinear FEM", *J. Central South Univ.*, **20**, 2263-2274.
- Londe, P. (1973), Analysis of the stability of rock slopes", *Quarterly J. Eng. Geology Hydrogeology*, **1**, 93-127.
- Mahmoudi, P.P., Mirzabozorg, H., Varmazyari, M. and Aghajanzadeh, S.M. (2016), "Effect of foundation nonlinearity on seismic response of an existing arch dam", *Civil Eng. J.*, **2**(5), 197-207.
- Mills-Bria, B.L., Nuss, L.K., & Chopra, A. K. (2008). *Current methodology at the Bureau of Reclamation for the nonlinear analyses of arch dams using explicit finite element techniques*. Paper presented at the The 14th World Conference on Earthquake Engineering October.
- Mirzabozorg, H., Ghaemian, M. and Roohezamin, A. (2019), "The reason of cracking in bottom gallery of SefidRud Buttress Dam and earthquake and post earthquake performance", *Struct. Monit. Maint.*, **6**(2), 103-124.
- Mirzabozorg, H., Varmazyari, M., Hoseini, M. and Gharebaghi, A.S. (2015), "A comparative study of rock wedge stability of an arch dam abutment subjected to static and seismic loading", *Soil Mech. Foundation Eng.*, **52**(5).
- Moradloo, J., Ahamdi, M. and Vahdani, S. (2008), "Nonlinear dynamic analysis of concrete arch dam considering large displacements", *Proceedings of the 14th World Confer. Earthquake Engineering, Beijing*.
- Mostafaei, H. and Behnamfar, F. (2019), *Stability Analysis of Arch Dam Abutments Due to Vertical Seismic Excitation*, Paper presented at the 8th International Conference on Seismology & Earthquake Engineering, Tehran, Iran.
- Mostafaei, H., Gilani, M.S. and Ghaemian, M. (2017), *The Effect of Grout Curtain Efficiency on Abutments Stability of an Arch Dam*, Paper presented at the 4th International Conference on Long-Term Behavior and Environmentally Friendly Rehabilitation Technologies of Dams Tehran, Iran.
- Mostafaei, H., Gilani, M.S. and Ghaemian, M. (2018), "A Comparative Study between Pseudo-static and Dynamic Analyses on Rock Wedge Stability of an Arch Dam", *Civil Eng. J.*, **4**(1), 179-187.
- Mostafaei, H., Sohrabi Gilani, M. and Ghaemian, M. (2017), "Stability analysis of arch dam abutments due to seismic loading", *Scientia Iranica A*, **24**(2), 292-300.
- Noble, C.R. and Nuss, L.K. (2004), *Nonlinear seismic analysis of Morrow Point dam*, Paper presented at the 13th World Conference on Earthquake Engineering, Vancouver, Canada.
- Pan, J. and Wang, J. (2019), "Effect of abutment movements on nonlinear seismic response of an arch dam", *Struct. Infrastruct. Eng.*, 1-15.
- PEER strong ground motion database. <<http://peer.berkeley.edu/smcat/search>> (2000).
- Sohrabi Gilani, M., Feldbacher, R. and Zenz, G. (2009), *Stability of dam abutment including seismic loading*. Paper presented at the 10th ICOLD Benchmark Workshop, Paris.
- Takaloozadeh, M. and Ghaemian, M. (2014), "Shape optimization of concrete arch dams considering abutment stability", *Scientia Iranica. Transaction A, Civil Eng.*, **21**(4), 1297.
- USACE (1994), Engineering and design: arch dam design, *EM 1110-2-2201*.

- USACE (2007), Earthquake design and evaluation of concrete hydraulic structures, *EM 1110-2-6053*.
- Wang, H. and Li, D. (2007), "Experimental study of dynamic damage of an arch dam", *Earthq. Eng. Struct. D.*, **36**(3), 347-366.
- Wang, J.T., Jin, F. and Zhang, C.H. (2019), "Nonlinear Seismic Response Analysis of High Arch Dams to Spatially-Varying Ground motions", *Int. J. Civil Eng.*, **17**(4), 487-493.
- Yu, I.N., Huang, S.K., Loh, K.J. and Loh, C.-H. (2019), "Application of subspace identification on the recorded seismic response data of Pacoima Dam", *Struct. Monit. Maint.*, **6**(4), 347-364.
- Zeinizadeh, A., Mirzabozorg, H., Noorzad, A. and Amirpour, A. (2018), *Hydrodynamic pressures in contraction joints including waterstops on seismic response of high arch dams*, Paper presented at the Structures.
- Zenz, G., Goldgruber, M. and Feldbacher, R. (2012), "Seismic stability of a rock wedge in the abutment of an arch dam", *Geomech. Tunnel.*, **5**, 186-194.
- Zhang, C., Xu, Y., Wang, G. and Jin, F. (2000), "Non-linear seismic response of arch dams with contraction joint opening and joint reinforcements", *Earthq. Eng. Struct. D.*, **29**(10), 1547-1566.
- Zhang, Q.L., Li, D.Y., Hu, C. and Hu, L. (2019), "Numerical Investigation into Underwater Explosion-Resistant Performance of an Arch Dam Considering Its Transverse Contraction and Control Joints", *J. Perform. Constr. Fac.*, **33**(6), 04019078.
- Zia, P. (1961), *Torsional strength of prestressed concrete members*, Paper presented at the Journal Proceedings.
- Ziaei, A., Ahangari, K., Moarefvand, P. and Mirzabozorg, H. (2017), "Extensometers results correction in concrete dams: A case study in RCC Zhavveh Dam", *Struct. Monit. Maint.*, **4**(1), 17-31.